Int. J. Electrochem. Sci., 12 **(2017)** 10084 – 10094, doi: 10.20964/2017.11.12

International Journal of
ELECTROCHEMICAL
SCIENCE
www.electrochemsci.org

Short Communication

A Study on Corrosion of VM125HC in simulated oilfield water

Shuliang Wang[1], *Feng Wang*[1], *Fei Xu*[1], *Mingyu Bao*[1], *Li Liu*[1,*], *Xin Wang*[1,*], *Chengqiang Ren*[1,2]

[1]School of Materials Science and Engineering, Southwest Petroleum University, 8 Xindu Avenue, Chengdu, Sichuan 610500, China
[2]State Key Laboratory of Oil and Gas Reservoir Geology and Exploitation, Southwest Petroleum University, 8 Xindu Avenue, Chengdu, Sichuan 610500, China
[*]E-mail: liuliswpu@163.com, xin.wang@swpu.edu.cn

Received: 8 July 2017 / *Accepted:* 27 August 2017 / *Published:* 12 October 2017

VM125HC steel is a new anti-collapse tube steel that was developed by V&M company. Up to date, there are very few studies reported regarding the corrosion mechanism of VM125HC steel. This work studied the corrosion mechanism of VM125HC in simulated oilfield water with saturated CO_2 by XRD, EDS, SEM, polarization curves and EIS. The results show that the corrosion rate of VM125HC in designated condition is affected by time. The pH value has played an important role in the process of the cathode reaction. The corrosion product films, composed of small $FeCO_3$ grain, are smooth. With the increase of immersion time, the corrosion films became denser, which enhanced the protective effect.

Keywords: VM125HC steel, CO_2 corrosion, Corrosion mechanism, Corrosion products film, Electrochemical

1. INTRODUCTION

Oil casing tube is an essential device in petroleum drilling process [1]. At present, as two of the most frequently used metal materials, N80 steel and P110 steel are widely found in the manufacturing of casing tubes all over the world [2, 3].

The mechanical properties of N80 steel and P110 steel are generally better than other analogues, making them suitable for exploitation of oil and gas drilling. With the increasing demand for oil and gas resources, the exploitation becomes more challenging, deep well or even ultra-deep well drilling are more commonly seen and sometimes inevitable. Ultra-deep well casing tube needs to sustain more load and annulus pressure, which requires tube steel with higher strength. The predominant N80 and P110 casing tube steels are unable to meet this demand anymore, so a new

casing tube steel with higher strength, namely VM125HC, was developed by V&M. However, the damage of the oil casing tube steel is not merely caused by the loads, but also the corrosion mediums from the environment under the well, such as the acid gas and the ions.

The VM125HC steel is not an acid-resistant steel. At high temperature and high pressure, the drilling media are strongly corrosive to the casing tube [4, 5], causing them to become thinner due to general corrosion and pitting corrosion. This poses serious safety issue to the tube [6]. The corrosion mechanism of CO_2 on metal has been studied by many researchers in recent years, including the corrosion behaviors of N80 steel and P110 steel [7-11]. It was found that the corrosion behavior is mainly influenced by the temperature, the CO_2/H_2S partial pressure, the flow conditions, the protective corrosion scales and the ion species and their concentration. In most cases, more than one factor is found to account for the corrosion simultaneously. In their investigations, the common methods to study corrosion behavior are weight loss method, potentiodynamic polarization curves, electrochemical impedance spectroscopy (EIS), scanning electron microscope (SEM), energy dispersive Spectrometer (EDS) and X-ray diffraction (XRD) [12-15]. Though there are many studies about N80 steel and P110 steel, the research of corrosion behavior about VM125HC steel is still lacking.

Thus, this work aims at the investigation of the corrosion mechanism of VM125HC in CO_2 solution, to examine the corrosion behavior of this useful yet not well-studied type of steel. The experiments investigate the corrosion mechanism of VM125HC and the mechanism of the formation of corrosion product films by weight loss method, potentiodynamic polarization curves, electrochemical impedance spectroscopy, SEM, EDS and XRD.

2. EXPERIMENTAL

2.1 Material and environment

All specimens used in this work were cut from VM125HC steel. Samples for weight loss tests, SEM, EDS and XRD were machined to dimensions of 50 mm×10 mm×3 mm (length, width, thickness), and others for electrochemical tests were machined to dimension of 10 mm×10 mm×3 mm (length, width, thickness). The chemical compositions of the steel are shown in Table 1. Prior to experiment, the specimens were polished subsequently up to 1000 grit silicon carbide paper, to obtain a fine surface and minimize the errors caused by surface roughness. The surface was then rinsed with distilled water and degreased with acetone, followed by cleaning and drying before weight.

Table 1. Chemical compositions of VM125HC steel (weight fraction, %)

Element	C	Si	Mn	Ni	Cr	Mo	Ti	Fe
Content (wt. %)	0.31	0.25	0.96	0.02	0.95	0.41	0.01	Balance

The experiment was operated in an autoclave, where the solution inside is the simulated oilfield water. The chemical compositions of the simulated oilfield water are shown in Table 2. The temperature was controlled at 90 °C, and the pressure was maintained at constantly 4 MPa. In order to obtain oxygen-free atmosphere, N_2 was bubbled into the solution for more than 4 h. The immersion time was set for 24 h, 50 h, 72 h and 240 h.

Table 2. Chemical compositions of simulation oilfield water (mg/L)

Ion	HCO^{3-}	Cl^-	SO_4^{2-}	Ca^{2+}	Na^+ and K^+
Content (mg/L)	636.86	7773.48	536.02	453.25	4911.19

2.2 SEM, EDS and XRD

The microtopography of surface scale on the corroded samples was analyzed using a JSMM-6490LV scanning electron microscope (SEM). The elemental analysis of the corrosion product was done using an Energy Dispersive Spectrometer (EDS), and the phase analysis of the corrosion product was made with a DX-2000 X-ray diffractometer (XRD). Samples were cleaned with acetone to remove the surface contamination before measurements.

2.3 Electrochemical methods

EIS was tested by AUTOLAB, using a three-electrode system containing a work electrode with a working area of 1 cm^2, a silver-silver chloride reference electrode and a big area platinum counter electrode. The solution in the electrolytic cell is the simulated oilfield water. After deoxygenation with N_2 bubbling, the gas of CO_2 was purged into the solution till saturation before test. The temperature was kept at 25 °C. The VM125HC samples used in the test of polarization curves were grinded and polished. The range of potential was from -0.4 V to -1.0 V, and the polarization curves were measured at a scan rate of 0.5 mV/s from the corrosion potential. The EIS measurements were carried out at open-circuit potential using an alternating current voltage with an amplitude of 10 mV and a frequency varying from 10^5 Hz to 10^{-2} Hz.

3. RESULTS AND DISCUSSION

3.1 Polarization measurements

The polarization curves of the VM125HC steel in the simulated oilfield water at 25°C are shown in Fig. 1, and the parameters of the weak polarization region after fitting are listed in Table 3. From Fig. 1 and Table 3, it is seen that the E_{corr} of VM125HC is -0.72 V and the I_{corr} is 5.66μA/cm^2.

In linear polarization region, the Tafel slope of cathode is 222.47, which is higher than that of the anode of 138.84. From the polarization curves, it is found that this is an active dissolution process, and there is no obvious passivation phenomenon in the anode.

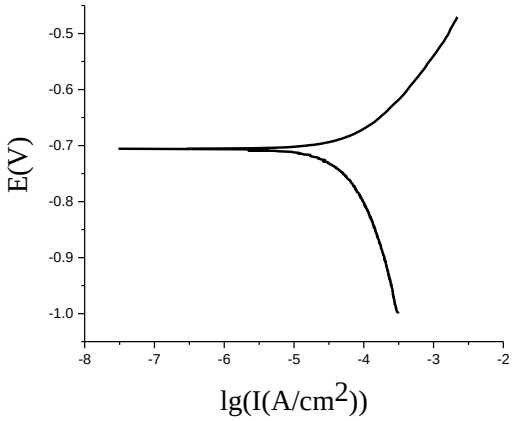

Figure 1. Potentiodynamic polarization curves of the VM125HC steel in the simulated oilfield water at 25°C.

Table 3. Fitted date of the weak polarization region in the polarization curves of the VM125HC steel in the simulated oilfield water at 25°C

	E_{corr} （V）	I_{corr} （μA/cm^2）	β_c (mV/dec)	β_a (mV/dec)
VM125HC	-0.72	5.66	-222.47	138.84

In the cathode process of CO_2 corrosion, the main reactions are as follows:

$$2H^+ + 2e \rightarrow H_2 \quad (1)$$

$$2H_2CO_3 + 2e \rightarrow H_2 + 2HCO_3^- \quad (2)$$

If the value of pH in the solution or the partial pressure of CO_2 is lower, the reactions will occur as follows:

$$2H_2O + 2e \rightarrow H_2 + 2OH^- \quad (3)$$

$$2HCO_3^- + 2e \rightarrow H_2 + 2CO_3^{2-} \quad (4)$$

The pH of the solution was tested to be 6, suggesting that the main reaction is reaction (2) [16, 17], where the cathode step of reaction rate control is determined by the diffusion and reduction of H^+.

3.2 Analysis of corrosion scales

Figure 2 shows the surface micromorphology of the samples after being corroded for 24 h, 72 h and 240 h respectively. In Fig. 2(a), the corrosion product is clearly visible on the surface of the sample. Fig. 2(b) is the SEM of corrosion product with 72 h of corrosion. On the surface, more

corrosion products formed, covering the surface of the sample. The surface is smooth with no obvious coarse grains. The micromorphology for the 240 h of corrosion is shown in Fig. 2(c) and is similar to that of the 72 h.

Zhao [18] studied the corrosion product of P110 steel (0.95wt. %Cr) immersed in CO_2 solution, and discovered that the value of pH had a significant impact on the micromorphology of the corrosion products. When the pH is greater than 7, there is compact $FeCO_3$ on the surface. While if the pH is below 7, no coarse grain appears on the surface. In this case, the morphology is similar with those in Fig. 2(b) and Fig. 2(c). Chen [19, 20] studied the corrosion product of N80 steel containing 1 wt. % and 4 wt. % of Cr in CO_2 solution and found the similar morphology. The main compositions were found to be crystalline $FeCO_3$ and noncrystalline $Cr(OH)_3$. Besides, the increase of the content of Cr will reduce the size of the $FeCO_3$. In this study, the content of Cr of the VM125HC steel is 0.95 wt. % (Table 1). Together with the morphology, it can be concluded that there is few noncrystalline $Cr(OH)_3$ in the corrosion product.

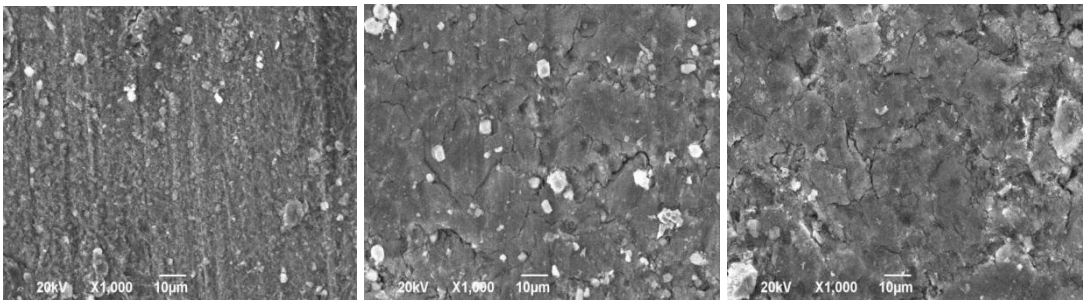

（a）24 h （b）72 h （c）240 h

Figure 2. Micromorphology of the corrosion products of VM125HC steel after different time of immersion in the simulated oilfield water in an autoclave at 90 °C with a pressure of 4 MPa.

The formation and development of $FeCO_3$ was the key of the formation of corrosion product films. If the formation of $FeCO_3$ was slow, the development of $FeCO_3$ would also become slow, which cannot ensure the formation of a compact corrosion layer and may even produce some holes on the surface [21]. On the other hand, because of the existence of $Cr(OH)_3$, which can fill the holes but cannot be able to form grains, which weakens the strength and adhesive force of the corrosion product films. Nevertheless, $Cr(OH)_3$ has selectivity on ions, which helps to stop the permeation behavior of anions from solution to the surface of the sample [22], thus weakens the cathodic reaction, and further weakens the corrosion.

XRD result of corrosion product films on VM125HC steel after 72 h of immersion in the simulated oilfield water in an autoclave at 90 °C with a pressure of 4 MPa was shown in Fig. 3. It is found that the main composition of the corrosion product films on VM125HC steel is $FeCO_3$. The peak in Fig. 3 may come from the pristine VM125HC. In the process of the formation of corrosion products, the reaction on the surface of the sample may occur as in reaction (5):

$$H_2CO_{3(aq)} + Fe \rightarrow FeCO_{3(aq)or(s)} + 2H_{2(g)} \quad (5)$$

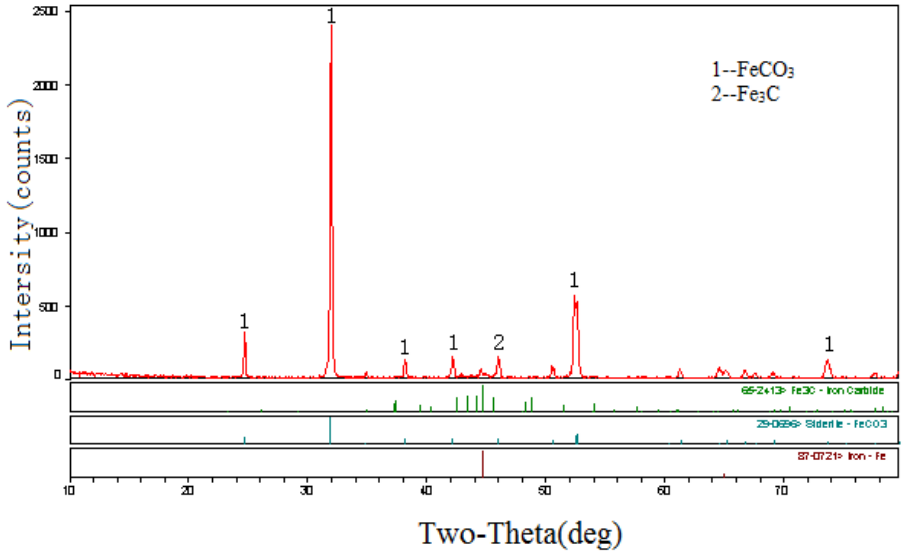

Figure 3. X-ray diffraction pattern of corrosion product films on VM125HC steel after 72 h of immersion in the simulated oilfield water in an autoclave at 90 °C with a pressure of 4 MPa

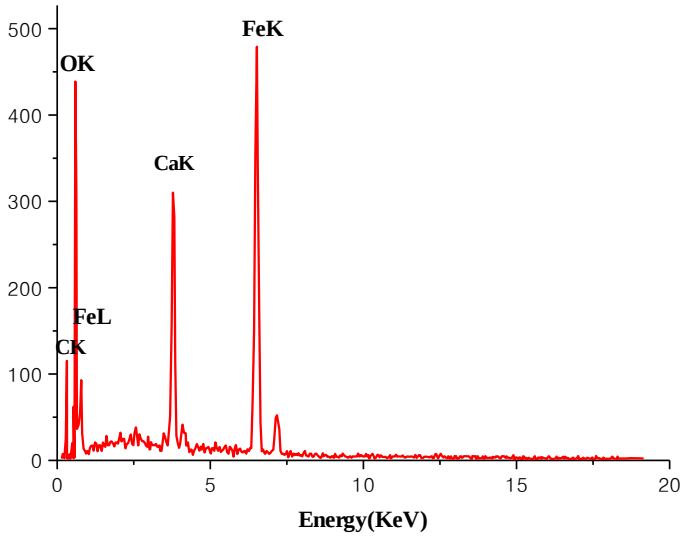

Figure 4. EDS pattern of corrosion product films on VM125HC steel after 72 h of immersion in the simulated oilfield water in an autoclave at 90 °C with a pressure of 4 MPa.

Figure 4 presents the EDS pattern of corrosion product films on VM125HC steel after 72 h immersion in the simulated oilfield water in an autoclave at 90 °C with a pressure of 4 MPa. Elements of Fe, Ca, C are found on the surface of the sample from the EDS pattern. Compound of Ca, however, is not found, possible because that the space of the element Fe in the lattice of $FeCO_3$ was occupied by element Ca, and then (Ca, Fe)CO_3 was formed [21]. Compound (Ca, Fe)CO_3 has a similar lattice parameter with $FeCO_3$, which overlaps with the $FeCO_3$ peak in XRD pattern.

3.3 Corrosion rate

The corrosion rate of metal was obtained by weight loss test. The corrosion rate, *v*, was calculated by equation (6):

$$v = \frac{8.76(m_0 - m_t)}{St\rho} \quad (6)$$

Where, m_0 and m_t are the weight of the sample before experiment and after removal of corrosion scale, respectively. *S* is the exposed surface area, *t* is the immersion time, and ρ is the density of the metal.

The average value of corrosion rate of VM125HC steel with different immersion time in the simulated oilfield water in an autoclave at 90 °C with a pressure of 4 MPa is shown in Fig. 5. It was found that the maximum average corrosion rate was reached with 24 h of immersion time. At 72 h, the corrosion rate decreased rapidly, but with little change at 120 h and 240 h of immersion time.

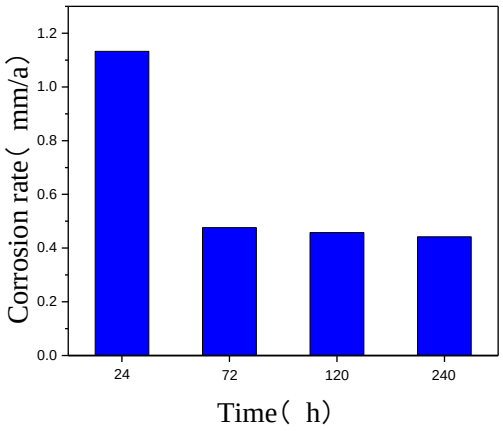

Figure 5. Average value of corrosion rate of VM125HC steel with different immersion time in the simulated oilfield water in an autoclave at 90 °C with a pressure of 4 MPa.

The experimental results from Sun [23] showed that the ferrite and cementite in the surface of the sample would form a couple, which induced the galvanic corrosion. Because the electrode potential of ferrite is lower than that of the cementite, the anodic cell will be dissolved preferentially, leaving the cementite in the surface. With the increase of the surface area where the cementite contacts with the solution, the dissolution of ferrite will be promoted during a period of time. Therefore in the early corrosion stage (such as 24 h), the sample has the maximum corrosion rate.

When the concentration of Fe^{2+} and CO_3^{2-} near the surface of the product is more than that of $FeCO_3$, Fe^{2+} and CO_3^{2-} will begin to form crystal and gradually cover the surface, as shown in Fig. 4(a). A compact corrosion product film will hinder the transfer of ions between the surface of the sample and the solution, thereby reducing the corrosion rate. However, the defects and pores in the corrosion products film will become the channel for the ion transferring, thus the sample will be corroded at a smaller rate. This explains when the time exceeded 72 h or more, there was little change in the average corrosion rate.

3.4 Analyses of EIS

After several days of corrosion, EIS were tested and recorded. The Nyquist plots and Bode plots for 3 days and 10 days of corrosion are shown in Fig. 6 and Fig. 7, respectively.

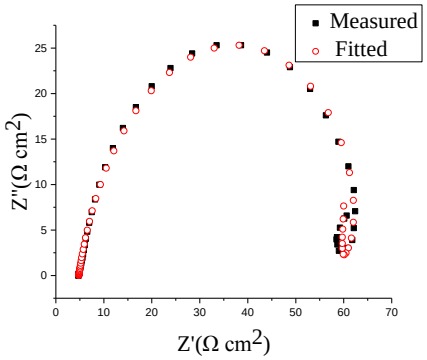

(a) Nyquist plot

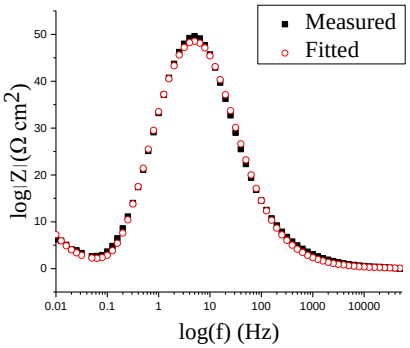

(b) Bode plot

Figure 6. EIS of VM125HC steel after 72 h of immersion in simulated oilfield water with saturated CO_2 at 25 °C: (a)Nyquist plot, (b) Bode plot.

Table 4 shows the EIS parameters fitted by ZSimpWin software. All the EIS plots show three arcs, which are related to three diverse time constants. The three arcs are high-frequency capacitance loop, low-frequency inductance loop and low-frequency capacitance loop, capacitance loop from high frequency to low frequency range, respectively. The corresponding Bode phase plots are shown as high-frequency peak, low-frequency valley and low-frequency peak.

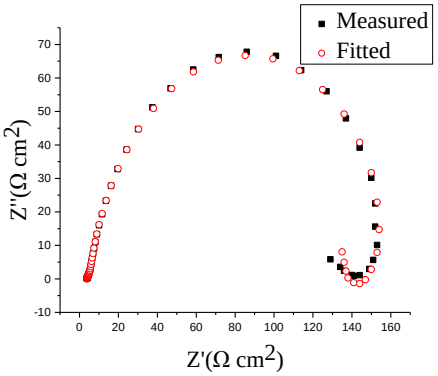

(a)Nyquist plot

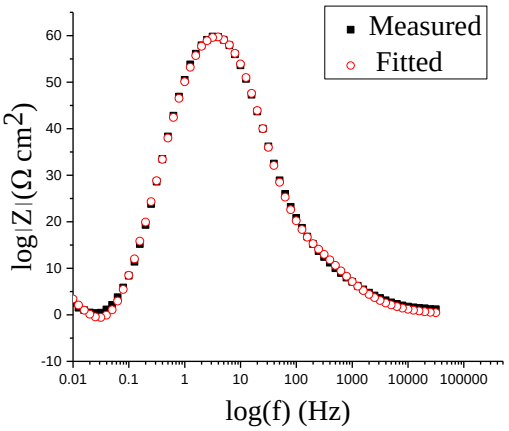

(b)Bode plot

Figure 7. EIS of VM125HC steel after 240 h immersion in simulation oilfield water with saturated CO_2 at 25 °C: (a)Nyquist plot, (b)Bode plot.

The equivalent circuit model for the corrosion system is shown in Fig. 8, where, R_s is the solution resistance, Q_f (CPE) is the constant phase element with corrosion product film, R_t is the resistance of the holes in the corrosion product films, R_L is the inductive resistance, L is the inductive impedance caused by electrode wires at high frequency and shows a very weak signal which can be ignored, Q_{dl} (CPE) is the constant phase element of electrical double layer, and R_{dl} is the charge transfer resistance of electrical double layer.

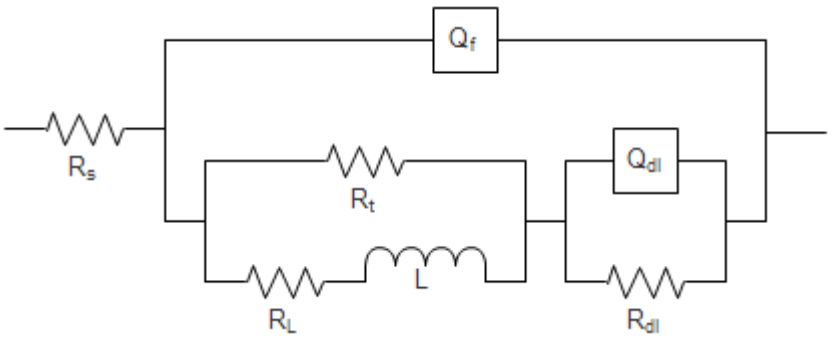

Figure 8. Equivalent circuit diagram after fitting of the EIS pattern.

Table 4. Component parameters in the Equivalent circuit diagram.

	R_s ($\Omega \cdot cm^{-2}$)	Q_f ($\Omega^{-1} \cdot cm^{-2} \cdot s^{-n}$)	n	R_t ($\Omega \cdot cm^{-2}$)	R_L ($\Omega \cdot cm^{-2}$)	L ($H \cdot cm^{-2}$)	Q_{dl} ($\Omega^{-1} \cdot cm^{-2} \cdot s^{-n}$)	n	R_{dl} ($\Omega \cdot cm^{-2}$)
3 days	4.836	3.329	0.832	66.86	316.1	340.4	2074	0.9918	10560
10 days	4.836	2.3	0.880	163.9	842.5	2556	6743	1	90100

In Table 4, the value of the R_t was increased from 66.86 Ω/cm^2 to 163.9 Ω/cm^2, which is the result of the corrosion product films becoming thicker and more compact, making the holes of the film smaller and the route longer. This causes the R_t to have an obviously increase.

In the investigation of Bockris [24], there will continuously be an intermediate process in the process of ferrite dissolving when $FeOH_{ads}$ would appear. In this process, the main reactions are as follows:

$$Fe + H_2O \leftrightarrow FeOH_{ads} + H^+ + e \quad (7)$$

$$FeOH_{ads} \rightarrow FeOH^+_{ads} + e \quad (8)$$

$$FeOH^+_{ads} + H^+ \leftrightarrow Fe^{2+} + H_2O \quad (9)$$

The dissolution process of anodic in the surface of the metal is shown above. This made the impedance arc appeared in the Nyquist plot. Furthermore, R_L and L are directly related to the cover of $FeOH_{ads}$ which has the adsorbability [25, 26]. After ten days, the value of R_L and L significantly increased, indicating that the content of $FeOH_{ads}$ in the holes is higher, and that the samples were dissolved sequentially, which increased the content of Fe^{2+} in the holes.

The impedance of the electric double layer on the surface of the metal and the resistance of charge transfer are related to the concentration of the solution near the surface of the metal [27]. Due to the strengthened blocking effect, the ion concentration near the electric double layer increased, leading to an increase of Q_{dl} and R_{dl}.

4. CONCLUSIONS

The corrosion mechanism of VM125HC steel in CO_2 solution was investigated. The value of pH was found to play an important role in the process of the cathode reaction. The corrosion product films, composed of small $FeCO_3$ grains as well as a small amount of amorphous $Cr(OH)_3$, are fairly smooth with nearly no change even after 72 h of immersion. The corrosion rate was large at the initial stage, but remained unchanged with immersion time, though the corrosion process was continued.

ACKNOWLEDGEMENTS

This work was financially supported by the National Natural Science Foundation of China (No. 51374 180), Scientific Research Foundation and Opening Foundation (X151516KCL24) of Southwest Petrole um University, National Undergraduate Training Program for Innovation and Entrepreneurship (20161 0615034). The authors also acknowledge a research funding from the Education Department of Sichua n Province (No. 17ZA0419), as well as start-up funding from Southwest Petroleum University.

References

1. A. Mohammed, C.J. Okeke, I. Abolle-Okoyeagu, *Comput. Chem. Eng*., 18 (1994) 349.
2. S.D. Zhu, A.Q. Fu, J. Miao, *Corros. Sci.*, 53 (2011) 3156.
3. J.L. Li, H.X. Ma, S.D. Zhu, *Corros. Sci.*, 86 (2014) 101.
4. M. Pour-Ghaz, O.B. Isgor, P. Ghods, *Corros. Sci.*, 51 (2009) 426.
5. L. Zhang, J. Yang, J. Sun, *Mater. Eng. Perform.*, 32 (2009) 87.
6. M.Y. Bao, C.Q. Ren, M. Lei, *Corros. Sci.*, 112 (2016) 585.
7. B.R. Linter, G.T. Burstein, *Corros. Sci.*, 41 (1999) 117.

8. Y. Zhang, X. Pang, S. Qu, *Corros. Sci.*, 59 (2012) 186.
9. P.C. Okafor, C.B. Liu, Y.J. Zhu, *Ind. Eng. Chem. Res.*, 50 (2011) 7273.
10. G.A. Zhang, D. Liu, Y.Z. Li, *Corros Sci.*, 120 (2017) 107.
11. Z. Sun, A. Singh, X. Xu, Res. *Chem. Intermed.*, 10 (2017).
12. X. Su, J.B. Sun, C. Sun, *Adv. Mater. Res.*, 816 (2013) 54.
13. J.B. Li, X. Hou, M.S. Zheng, *Int. J. Electrochem. Sci.*, 2 (2007) 607.
14. X. Jiang, Y.G. Zheng, W. Ke, *Corros. Sci.*, 47 (2005) 2636.
15. A.M. Abdel-Gaber, B.A. Abd-El-Nabey, I.M. Sidahmed, *Corros. Sci.*, 48 (2006) 2765.
16. M.B. Kermani, A. Morshed, *Corrosion.*, 59 (2003) 659.
17. S. Nešić, Corros. *Sci.*, 49 (2007) 4308.
18. J.M. Zhao, Y. Lu, H.X. Liu, *Corros. Eng. Sci. Technol.*, 43 (2008) 313.
19. C.F. Chen, M.X. Lu, G.X. Zhao, *Acta Metall.*, 39 (2003) 2219.
20. Z.Q. Bai, C.F. Chen, M.X. Lu, *Appl. Surf. Sci.*, 252 (2006) 7578.
21. M. Gao, X. Pang, K. Gao, *Corros. Sci.*, 53 (2011) 557.
22. C.A. Palacios, J.R. Shadley, *Corrosion.*, 47 (1991) 122.
23. J.B. Sun, G.A. Zhang, W. Liu, M.X. Lu, *Corros. Sci.*, 57 (2012) 131.
24. J.M. Bockris, D. Drazic, *Electrochim. acta.*, 7 (1962) 293.
25. P. Li, T.C. Tan, J.Y. Lee, *Corros. Sci.*, 38 (1996) 1935.
26. G.A. Zhang, Y.F. Cheng, *Corros. Sci.*, 51 (2009) 1589.
27. F. Farelas, M. Galicia, B. Brown, *Corros. Sci.*, 52 (2010) 509.